Frontiers of Physics
https://doi.org/10.1007/s11467-021-1079-4
Front. Phys.
16(6), 63500 (2021)

RESEARCH ARTICLE

Pseudo-copper Ni–Zn alloy catalysts for carbon dioxide reduction to C_2 products

Xiao-Dong Zhang[1], Kang Liu[1], Jun-Wei Fu[1], Hong-Mei Li[1], Hao Pan[2], Jun-Hua Hu[3], Min Liu[1,†]

[1] *School of Physics and Electronics, State Key Laboratory of Powder Metallurgy, Central South University, Changsha 410083, China*
[2] *Department of Periodontics & Oral Mucosal Section, Xiangya Stomatological Hospital, Central South University, Changsha 410008, China*
[3] *School of Materials Science and Engineering, Zhengzhou University, Zhengzhou 450002, China*
Corresponding author. E-mail: [†] *minliu@csu.edu.cn*
Received February 1, 2021; accepted April 16, 2021

Electrocatalytic CO_2 reduction reaction (CO_2RR) to obtain C_2 products has drawn widespread attentions. Copper-based materials are the most reported catalysts for CO_2 reduction to C_2 products. Design of high-efficiency pseudo-copper catalysts according to the key characteristics of copper (Cu) is an important strategy to understand the reaction mechanism of C_2 products. In this work, density function theory (DFT) calculations are used to predict nickel–zinc (NiZn) alloy catalysts with the criteria similar structure and intermediate adsorption property to Cu catalyst. The calculated tops of 3d states of $NiZn_3(001)$ catalysts are the same as Cu(100), which is the key parameter affecting the adsorption of intermediate products. As a result, $NiZn_3(001)$ exhibits similar adsorption properties with Cu(100) on the crucial intermediates $*CO_2$, *CO and *H. Moreover, we further studied CO formation, CO hydrogenation and C–C coupling process on Ni–Zn alloys. The free energy profile of C_2 products formation shows that the energy barrier of C_2 products formation on $NiZn_3(001)$ is even lower than Cu(100). These results indicate that $NiZn_3$ alloy as pseudo-copper catalyst can exhibit a higher catalytic activity and selectivity of C_2 products during CO_2RR. This work proposes a feasible pseudo-copper catalyst and provides guidance to design high-efficiency catalysts for CO_2RR to C_2 or multi-carbon products.

Keywords pseudo-copper catalysts, surface and electronic structure, adsorption abilities, Ni–Zn alloys, CO_2RR C_2 products, DFT

1 Introduction

The excessive consumption of fossil fuels dramatically increases CO_2 concentration in the atmosphere and results in global warming and energy crisis. Developing and utilizing renewable energy sources to optimize the energy structure have received widespread attention [1–6]. Electrocatalytic or photocatalytic CO_2 reduction reactions (CO_2RR) can convert intermittent electricity or solar energy into available chemical energy [7–11], and accelerate the carbon cycle. CO_2RR to obtain C_2 products (ethylene [12–14] and ethanol [15–17], etc.) with higher energy density than C_1 products has become the focus in the energy catalysis field [18, 19]

Copper-based (Cu-based) materials are the most widely reported CO_2 reduction catalysts to generate C_2 products [19–21], due to its unique surface structure [22–24] electronic structure [25–29] and intermediate adsorption ability [30–33]. Many researches focus on improving the Faradic efficiency (FE) of C_2 products by forming Cu-based alloys, such as Cu–Ag [34, 35] and Cu–Zn [36, 37] alloys. In addition, other non-copperbased alloys (Ni–Al [38, 39] Ni-Ga [39, 40] and Pd–Au [41] alloy) have been reported to produce low yield of C_2 products, which indicates the possibility of non-copper-based catalysts producing C_2 products. According to the key characteristics of copper-based catalysts for C_2 products to design high-efficiency pseudo-copper catalysts is an important strategy to enhance the activity and selectivity of C_2 products. There are two criteria for evaluating pseudo-copper catalysts to generate C_2 products: (i) Copper-like surface structure and electronic structure. Cu(100) with unique surface structure sensitivity [23, 24, 42] and electronic structure [25–29] can control the activity and selectivity toward C_2 products. (ii) Copper-like adsorption abilities of $*CO_2$, *CO and *H. These adsorption abilities are the

* This article can also be found at http://journal.hep.com.cn/fop/EN/10.1007/s11467-021-1079-4.

essential descriptors for CO_2 activation [43, 44] CO hydrogenation, C–C coupling [31, 32], and hydrogen evolution reaction (HER) [30, 33]. Based on above criteria, design of pseudo-copper catalysts with high-efficiency C_2 products is promising and significant.

Alloying is a feasible strategy for obtaining pseudo-copper catalysts [45], because the alloying effect is an effective method to regulate the adsorption abilities, surface and electronic structure of metal-based catalysts [38, 46]. The surface and electronic structure are primary consideration of component metals in pseudo-copper alloy catalysts. Nickel (Ni) and Zinc (Zn) are adjacent to Cu in the periodic table of elements. Ni has the face-centered cubic (fcc) lattice similar with Cu and its 3d states is adjustable [29]. Zn exhibits excellent potential in adjusting electronic structure of alloy catalysts [47]. Ni–Zn alloy can exhibit a similar electron/atom (e/a) ratio with Cu, which indicates that Ni–Zn alloy will have a stable copper-like lattice structure [48]. In addition, the electronic structure and intermediate adsorption ability of Ni–Zn alloys can be tuned by interaction between Ni and Zn. Ni–Zn alloys with copper-like surface and electronic structure, and intermediate adsorption ability are potential to obtain C_2 products in CO_2RR.

In this work, NiZn(110) and $NiZn_3$(001) are selected as the active facets due to their similar square geometric site structure to Cu(100). The CO_2 formation and C–C coupling on NiZn(110) and $NiZn_3$(001) are further investigated to analyze the feasibility of C_2 products. The free energy profiles of C_2 products formation are used to study the reaction mechanism of NiZn(110) and $NiZn_3$(001). The calculated results indicate that the NiZn and $NiZn_3$ alloys exhibit copper-like properties with these critical criteria. The energy barrier of C_2 products formation on $NiZn_3$(001) is even lower than Cu(100). Therefore, the NiZn and $NiZn_3$ alloys are potential pseudo-copper catalysts for CO_2 reduction to C_2 products. This work proposes a feasible pseudo-copper catalyst and provides guidance to design high-efficiency catalysts for CO_2RR to C_2 or multi-carbon products.

2 Computational methods

The Vienna *Ab initio* Simulation Package (VASP) was used to perform spin-polarized DFT [49–51]. The projector augmented wave (PAW) method was applied to describe the effective potential between the ion core and the electrons. The generalized gradient approximation (GGA) with Perdew–Burke–Ernzerhof (PBE) functional was adopted to calculate the exchange-correlation energy [52]. We set the kinetic cutoff energy of the plane wave as 450 eV. The convergence criteria for force and energy were set as 0.02 eV·Å^{-1} and 10^{-5} eV per atom, respectively [53]. We built the (3 × 3 × 4) surface supercells for all slab models, including NiZn(110), NiZn(101), $NiZn_3$(001), $NiZn_3$(100), Cu(100) Cu(111), Ni(100), Ni(111), and Zn(001). The corresponding structures are shown in Fig. S1. For the Brillouin zone integration, we used a Monkhorst–Pack mesh with 3 × 3 × 1 K-points. The computational details of the adsorption energy and Gibbs free energy are shown in the Supporting Information.

3 Results and discussion

3.1 Surface and electronic structures

Cu(100) is proven to be the most favorable surface orientation for C–C coupling [22], which can be attributed to its square ensemble sites [23, 24]. Like Cu, NiZn and $NiZn_3$ alloys also have a face-centered tetragonal (fct) structure. As shown in Fig. S1, the NiZn(110), NiZn(101), $NiZn_3$(001), $NiZn_3$(100), Ni(100) and Zn(001) exhibit the similar square geometric site structure to Cu(100). Furthermore, Table S1 compares the calculated lattice constants of these facets. The lattice constants of Cu(100) were calculated to be $a = b = 11.04$ Å, while the Ni(100) and Zn(001) were $a = b = 10.53$ Å and $a = b = 11.25$ Å, respectively. This structural difference makes a big difference in catalytic performance. Interestingly, the lattice constants of NiZn(110) ($a = 9.80$ Å, $b = 11.59$ Å) and $NiZn_3$(001) ($a = b = 11.01$ Å) are more closer to Cu(100) [Fig. 1(a)] due to the structure rearrangement of Zn on Ni in alloy phases. The basic site configuration of NiZn(110) and $NiZn_3$(001) can be same as that of Cu(100), which has a great influence on the whole catalytic C_2 formation reaction process.

As shown in Fig. 1(b), the d-band of Cu(100) mainly distributes below the Fermi level (E_F), and its top of the 3d states are located around –1.8 eV. The anti-bonding states are filled for Cu(100), which leads to Cu(100) has favorable adsorption for key intermediates [28]. As for Ni(100), the d-band cross the E_F and part of the anti-bonding states is empty for Ni(100), which will lead to strong adsorption abilities of intermediates and not conducive to further activation of adsorbate [29]. The d-band of Zn(001) mainly distributes at –8 eV, which results in too weak adsorption of intermediates. Both NiZn(110) and $NiZn_3$(001) exhibit copper-like electronic structure in the density of states (DOS) calculations. Moreover, the top of the 3d states of $NiZn_3$(001) is almost the same to Cu(100). These results suggest that the formation of the alloy with Zn efficiently bring the apparent depression of the 3d states of Ni near E_F, which makes the DOS of NiZn alloys similar to that of Cu.

The d-band position is closely related to the binding strength between intermediates and catalysts. In detail, the electronic interaction between the adsorbate and the 3d states lead to the formation of bonding and antibonding states [29, 54]. The lower position (relative to the

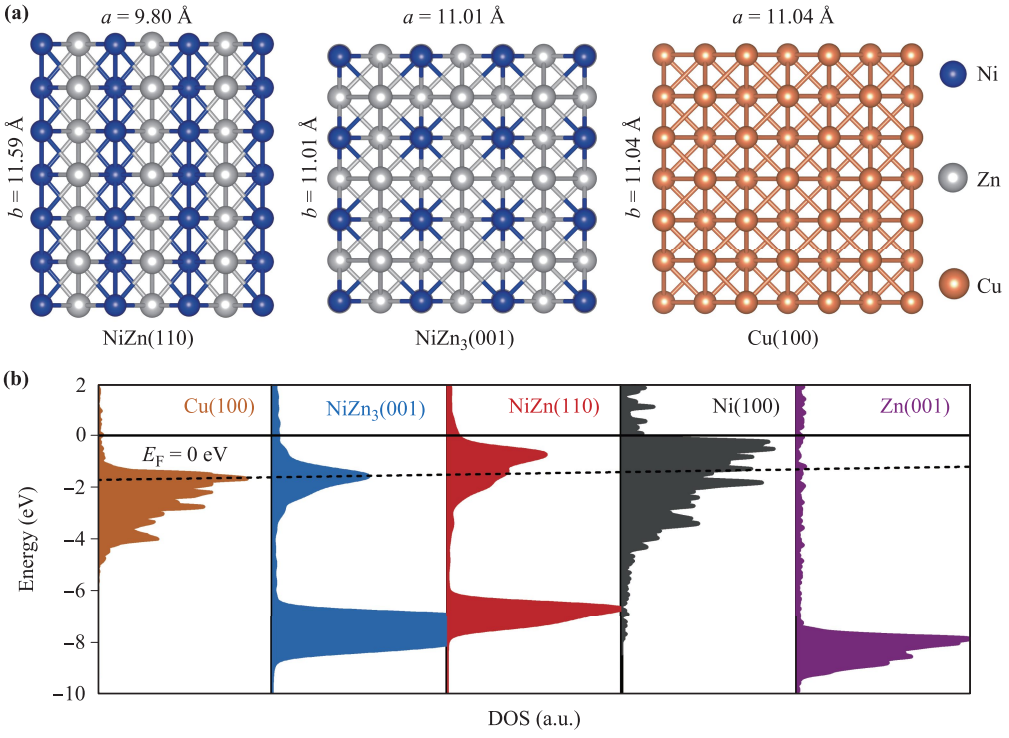

Fig. 1 **(a)** The top view of structure model on NiZn(110), $NiZn_3$(001) and Cu(100). **(b)** Calculated valence electronic DOSs at Cu(100), $NiZn_3$(001), NiZn(110), Ni(100) and Zn(001). The dotted line (–1.5 eV) was a guideline for comparing the positions of the d-band tops.

Fermi level) of the d-band, the weaker binding strength, due to the occupancy of anti-bonding states. Compared with Ni(100), the adjusted d-band positions of NiZn alloys indicate suitable adsorption properties of intermediates, similar to Cu(100), which is favorable to the further activation of intermediates (CO_2, CO), and avoiding CO poisoning or strong hydrogen evolution reactions (HER).

3.2 Adsorption abilities of *CO_2, *CO and *H

Copper-like adsorption abilities of *CO_2, *CO and *H are regarded as the key criterion to evaluate the potential catalytic performance of pseudo-copper catalysts. The adsorption abilities of *CO_2, *CO and *H directly influence the CO formation [43, 44] and C–C coupling [31, 32, 55, 56], and HER [30, 33], respectively. The adsorption energies of *CO_2, *CO and *H on different facets are shown in Table S2.

The CO_2 reduction process is accompanied by the competitive HER and hydrogenation process. The relationship between the adsorption energy of *H (ΔE_H) and reactants *CO_2 (ΔE_{CO_2}) and the relationship between ΔE_H and crucial intermediate *CO (ΔE_{CO}) both are very important. As shown in Fig. 2(a), the upper right region

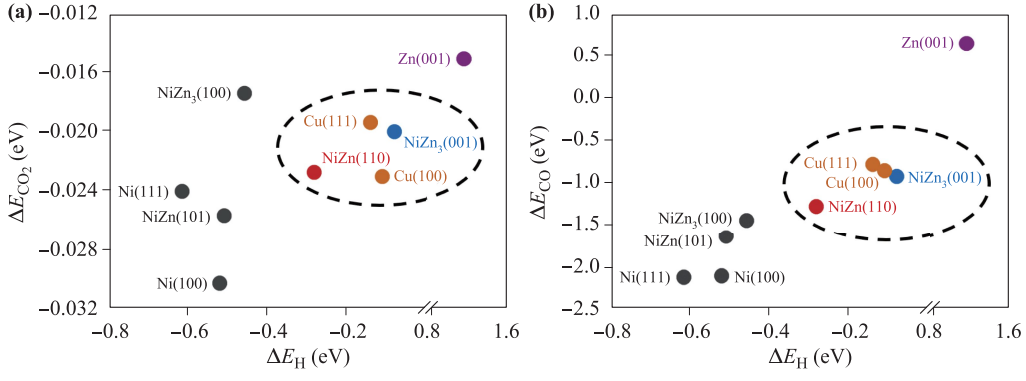

Fig. 2 (a) The relationship between the adsorption energy of *H (ΔE_H) and reactants *CO_2 (ΔE_{CO_2}), and **(b)** the relationship between ΔE_H and crucial intermediate *CO (ΔE_{CO}).

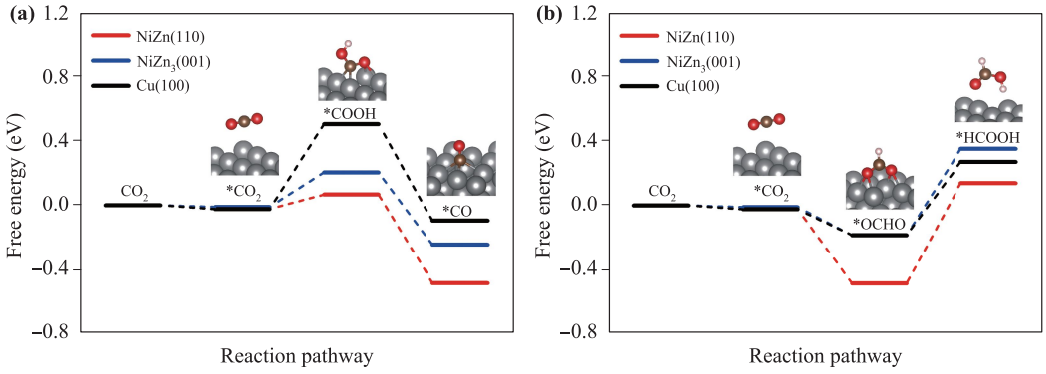

Fig. 3 Free energy profiles of the reaction pathway for **(a)** *CO formation and **(b)** *HCOOH formation on NiZn(110), $NiZn_3$(001) and Cu(100).

indicates that both the ΔE_{CO_2} and ΔE_H are weak, not conducive to the CO_2 reduction reaction. The lower left region indicates that ΔE_H is much stronger than ΔE_{CO_2}, which will lead to the active site being occupied by *H, and is not conducive to CO_2 activation. In the circle area, NiZn(110) and $NiZn_3$(001) exhibit copper-like $*CO_2$ and *H adsorption energies. Proper ΔE_{CO_2} and ΔE_H indicate the suitable coordination of CO_2 adsorption and CO_2 hydrogenation process, which provides the possibility for the generation of intermediate CO. The adsorption abilities of *CO and *H are shown in Fig. 2(b). Similarly, the upper right region indicates that both the ΔE_{CO} and ΔE_H are weak, not conducive to the CO hydrogenation and C–C coupling reaction. The lower left region indicates that both ΔE_{CO} and ΔE_H are strong, which will lead to CO poisoning and severe competing HER. In the circle area, NiZn(110) and $NiZn_3$(001) exhibit copper-like *CO and *H adsorption energies. Proper ΔE_{CO} and ΔE_H indicate the suitable coordination of CO hydrogenation and C–C coupling process, which provides the possibility for the generation of C_2 products.

The Cu-like adsorption abilities of NiZn(110) and $NiZn_3$(001) are mainly due to the fact that Zn adjusts the surface and electronic structure of Ni. By screening and evaluation, NiZn(110) and $NiZn_3$(001) are the potential pseudo-copper catalyst to generation C_2 products during CO_2RR.

3.3 Reaction pathway of *CO formation

CO is the key intermediate for the formation of C_2 products, and the first intermediate for CO formation from CO_2 is *COOH [44, 46] The reaction pathways of CO formation are analyzed on NiZn(110) and $NiZn_3$(001) [Fig. 3(a)]. The formation energy barriers of *CO (ΔG_{*CO}) on NiZn(110) and $NiZn_3$(001) are 0.09 eV and 0.21 eV, respectively, which both are much lower than Cu(100) (0.53 eV) (Table S3). The adsorptions of *COOH intermediate on NiZn(110) and $NiZn_3$(001) are much stronger than on Cu(100), which is the key factor of lower formation energy barriers of *CO on NiZn(110) and $NiZn_3$(001).

In addition, the competitive reaction of formate (*HCOOH) formation is also considered on NiZn(110) and $NiZn_3$(001) [Fig. 3(b)]. The formation energy barriers of formate (ΔG_{*HCOOH}) on NiZn(110) and $NiZn_3$(001) are 0.62 eV and 0.53 eV (Table S4), which is higher than formation energy barriers of *CO. This result indicates that the formation of *CO on NiZn(110) and $NiZn_3$(001) is easier than *HCOOH. As for Cu(100), the formation energy barriers of formate (ΔG_{*HCOOH}) is 0.45 eV, which is slightly lower than ΔG_{*CO} of 0.53 eV. It suggests that NiZn(110) and $NiZn_3$(001) have higher selectivity to *CO than Cu(100).

3.4 Reaction pathway of C–C coupling

C–C coupling is reported to be the crucial reaction for the C_2 formation [57]. There are three main pathways for the C–C coupling reaction [32] [Fig. 4(a)]: (i) *CO–CO intermediate formed via *CO coupling with $CO_{(g)}$; (ii) *CHO is formed via *CO hydrogenation, and coupling with $CO_{(g)}$ to form *CHO–CO intermediates; (iii) *CO hydrogenation to form *COH, then *COH hydrogenation to form $*CH_2$ intermediate, and the C–C bond formed via $*CH_2$ dimerization.

The formation energy barriers of three intermediates (*CHO, *COH and *CO–CO) during C–C coupling are calculated to study the C_2 product evolution. As shown in Table S5, both the free energy barriers of *COH and *CO–CO are much higher than *CHO. Therefore, *CHO–CO is considered as the main intermediates for C–C coupling reaction on NiZn(110), $NiZn_3$(001), and Cu(100)

In the *CHO–CO pathway, NiZn(110) and $NiZn_3$(001) show similar reaction trends to Cu(100) [Fig. 4(b)]. Compared with Cu(100) and NiZn(110), $NiZn_3$(001) has the lowest free energy barrier (0.60 eV) (Table S6) which can be attributed to the optimal Cu-like surface/electronic structure and intermediate adsorption abilities of $NiZn_3$(001). For NiZn(110), although it has

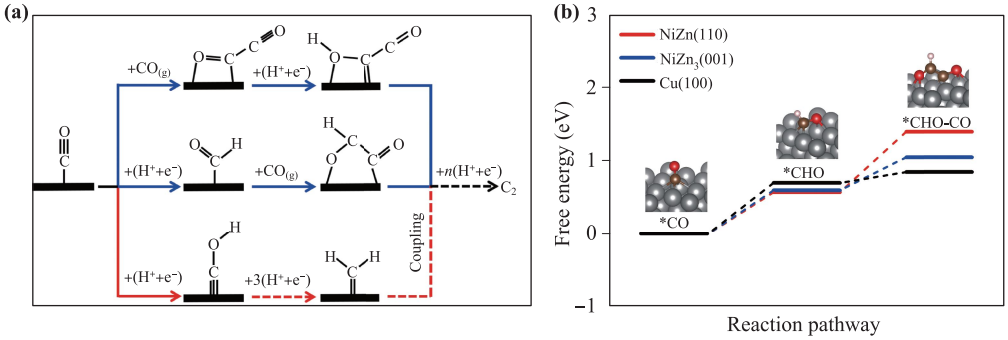

Fig. 4 **(a)** Schematic description of three main C–C coupling pathways from *CO intermediates. **(b)** Free energy profile of C–C coupling via *CHO–CO intermediate on NiZn(110), $NiZn_3$(001) and Cu(100).

the lowest free energy barrier of *CO → *CHO (0.57 eV), the energy barrier of *CHO → *CHO–CO is higher due to the strong *CO adsorption abilities on NiZn(110), which is detrimental to the C–C bond formation.

3.5 Reaction mechanism of C_2 products formation

To understand the reaction mechanism of C_2 products formation on NiZn(110) and $NiZn_3$(001), the C_2 intermediates in the reaction pathway from *CHO–CO to *CHO–CH are investigated. *CHO–CH is the crucial precursor of the C_2 product, and the *CHO–CH_2 intermediate formed by its hydrogenation is considered to be the bifurcation of the pathway for C_2H_4 and C_2H_5OH formation [32, 58].

Three possible pathways of *CHO–CO hydrogenation on NiZn(110), $NiZn_3$(001) and Cu(100) are considered: alternate (*CHO–CHO) (Fig. S2 and Table S7), hybrid (*CHO–COH) (Fig. S3 and Table S8) and distal (*CHOH-CO) (Fig. S4 and Table S9) pathways. The lowest free energies of *CHO–CH formation on $NiZn_3$(001) and Cu(100) both are alternate pathway[Fig. 5(b) and Fig. S5], while that on NiZn(110) is hybrid pathways [Fig. 5(a)].

The main formation mechanism of C_2H_4 and C_2H_5OH are formed via the deoxygenation and hydrogenation of *CHO–CH_2 intermediate, respectively. Figure 5(c) compares the free energies of the reaction pathway from CO_2 to *CHO–CH_2 on NiZn(110) (Fig. S6), $NiZn_3$(001) (Fig. S7), and Cu(100) (Fig. S8). In detail, the step of *CO hydrogenation is the rate determination step (RDS) on $NiZn_3$(001) and Cu(100), but the RDS on NiZn(110)

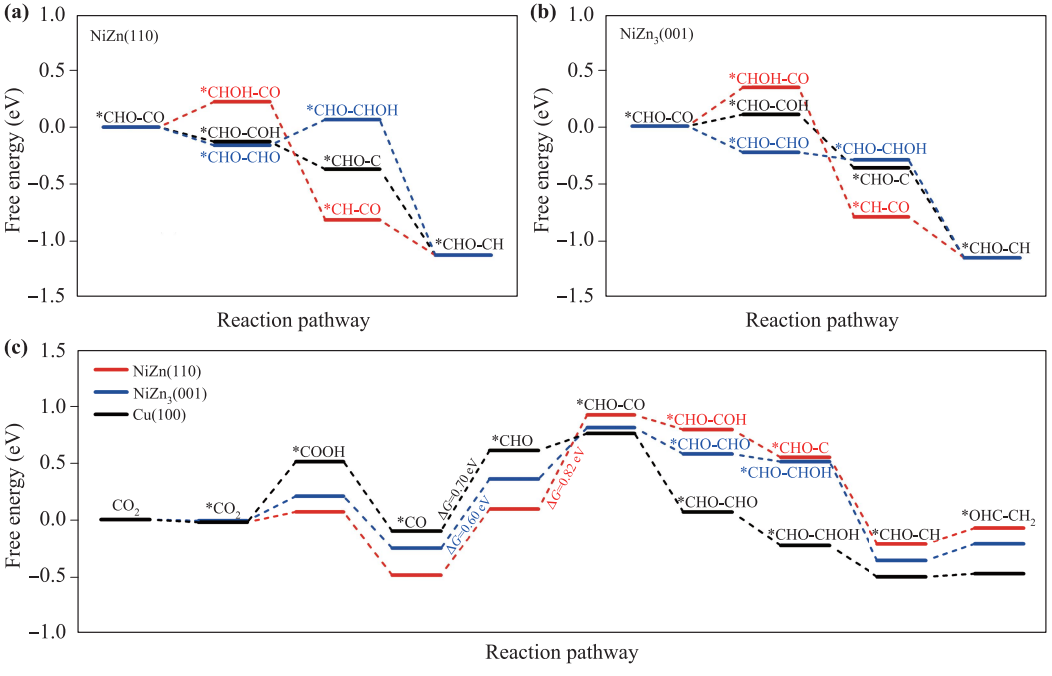

Fig. 5 The three pathways of *CHO–CO hydrogenation to *CHO–CH on **(a)** NiZn(110), and **(b)** $NiZn_3$(001). **(c)** The lowest free energy pathway for C_2 formation from CO_2 to *OHC–CH_2 on NiZn(100), $NiZn_3$(001) and Cu(100).

is the *CHO–CO formation via *CHO and *CO coupling. Moreover, $NiZn_3(001)$ shows the lowest energy barrier (0.60 eV) for CO_2RR to *CHO–CH_2, compare with Cu(100) (0.70 eV) and NiZn(110) (0.82 eV). This calculation result is consistent with the screening criteria. $NiZn_3(001)$ is an ideal pseudo-copper catalyst for CO_2 reduction to C_2 products.

4 Conclusion

In summary, we designed the Ni–Zn alloys as the promising pseudo-copper catalysts and predicated reaction mechanism for CO_2RR to C_2. DFT calculations revealed that NiZn and $NiZn_3$ had the two key criteria of pseudo-copper alloys: copper-like surface and electronic structure and intermediate adsorption abilities. $NiZn_3(001)$ alloy had lower free energy barrier (0.60 eV) than Cu(100) (0.70 eV) and NiZn(110) (0.82 eV) in the reaction from CO_2 to *CHO–CH_2, and the C–C bond was formed through the *CHO and CO coupling. The *CHO–CH_2 intermediate was preferred formed along the alternate hydrogenation pathway. Importantly, the copper-like nature of NiZn and $NiZn_3$ alloys were derived from the interaction of Ni and Zn, which tuned their lattice structure and 3d state toward Cu. Here, two critical criteria of the pseudo-copper catalyst are established to form C_2 products from CO_2, and provides guidance to design high-efficiency catalysts for CO_2RR to C_2 or multi-carbon products.

Electronic supplementary material Electronic supplementary materials are available in the online version of this article at https://doi.org/10.1007/s11467-021-1079-4 and http://journal.hep.com.cn/fop/EN/10.1007/s11467-021-1079-4 and are accessible for authorized users.

Acknowledgements The authors gratefully thank the National Natural Science Foundation of China (Grant Nos. 21872174, 22002189, and U1932148), the International Science and Technology Cooperation Program (Grant Nos. 2017YFE0127800 and 2018YFE0203402), the Hunan Provincial Science and Technology Program (No. 2017XK2026), the Hunan Provincial Natural Science Foundation (Grant Nos. 2020JJ2041 and 2020JJ5691), the Hunan Provincial Science and Technology Plan Project (No. 2017TP1001), the Shenzhen Science and Technology Innovation Project (No. JCYJ20180307151313532), the Key R&D Program of Hunan Province (No. 2020WK2002).

References

1. Z. Cui, W. Du, C. Xiao, Q. Li, R. Sa, C. Sun, and Z. Ma, Enhancing hydrogen evolution of MoS_2 Basal planes by combining single-boron catalyst and compressive strain, *Front. Phys.* 15(6), 63502 (2020)
2. K. Chen, H. Li, Y. Xu, K. Liu, H. Li, X. Xu, X. Qiu, and M. Liu, Untying thioether bond structures enabled by "voltage-scissors" for stable room temperature sodium-sulfur batteries, *Nanoscale* 11(13), 5967 (2019)
3. X. Li, Y. B. Zhao, F. Fan, L. Levina, M. Liu, R. Quintero-Bermudez, X. Gong, L. N. Quan, J. Fan, Z. Yang, S. Hoogland, O. Voznyy, Z. H. Lu, and E. H. Sargent, Bright colloidal quantum dot light-emitting diodes enabled by efficient chlorination, *Nat. Photon.* 12(3), 159 (2018)
4. Y. Wei, G. Xing, K. Liu, G. Li, P. Dang, S. Liang, M. Liu, Z. Cheng, D. Jin, and J. Lin, New strategy for designing orangish-red-emitting phosphor via oxygen-vacancy-induced electronic localization, *Light Sci. Appl.* 8(1), 15 (2019)
5. K. Chen, W. Fan, C. Huang, and X. Qiu, Enhanced stability and catalytic activity of bismuth nanoparticles by modified with porous silica, *J. Phys. Chem. Solids* 110, 9 (2017)
6. Q. Li, S. Qiu, and B. Jia, Theoretical investigation of $CoTa_2O_6$/graphene heterojunctions for oxygen evolution reaction, *Front. Phys.* 16(1), 13503 (2021)
7. Z. Q. Wang, T. Y. Lü, H. Q. Wang, Y. P. Feng, and J. C. Zheng, Review of borophene and its potential applications, *Front. Phys.* 14(3), 33403 (2019)
8. Y. H. Lui, B. Zhang, and S. Hu, Rational design of photoelectrodes for photoelectrochemical water splitting and CO_2 reduction, *Front. Phys.* 14(5), 53402 (2019)
9. J. Fu, K. Jiang, X. Qiu, J. Yu, and M. Liu, Product selectivity of photocatalytic CO_2 reduction reactions, *Mater. Today* 32, 222 (2020)
10. J. Fu, K. Liu, K. Jiang, H. Li, P. An, W. Li, N. Zhang, H. Li, X. Xu, H. Zhou, D. Tang, X. Wang, X. Qiu, and M. Liu, Graphitic carbon nitride with dopant induced charge localization for enhanced photoreduction of CO_2 to CH_4, *Adv. Sci.* 6(18), 1900796 (2019)
11. J. Fu, S. Wang, Z. Wang, K. Liu, H. Li, H. Liu, J. Hu, X. Xu, H. Li, and M. Liu, Graphitic carbon nitride based single-atom photocatalysts, *Front. Phys.* 15(3), 33201 (2020)
12. R. Kas, R. Kortlever, H. Yilmaz, M. T. M. Koper, and G. Mul, Manipulating the hydrocarbon selectivity of copper nanoparticles in CO_2 electroreduction by process conditions, *ChemElectroChem* 2(3), 354 (2015)
13. M. Zhong, K. Tran, Y. Min, C. Wang, Z. Wang, C. T. Dinh, P. De Luna, Z. Yu, A. S. Rasouli, P. Brodersen, S. Sun, O. Voznyy, C. S. Tan, M. Askerka, F. Che, M. Liu, A. Seifitokaldani, Y. Pang, S. C. Lo, A. Ip, Z. Ulissi, and E. H. Sargent, Accelerated discovery of CO_2 electrocatalysts using active machine learning, *Nature* 581(7807), 178 (2020)
14. R. Reske, M. Duca, M. Oezaslan, K. J. P. Schouten, M. T. M. Koper, and P. Strassert, Controlling catalytic selectivities during CO_2 electroreduction on thin Cu metal overlayers, *J. Phys. Chem. Lett.* 4(15), 2410 (2013)
15. F. Calle-Vallejo and M. T. Koper, Theoretical considerations on the electroreduction of CO to C_2 species on Cu(100) electrodes, *Angew. Chem. Int. Ed.* 52(28), 7282 (2013)

16. X. Wang, Z. Wang, F. P. García de Arquer, C. T. Dinh, A. Ozden, Y. C. Li, D. H. Nam, J. Li, Y. S. Liu, J. Wicks, Z. Chen, M. Chi, B. Chen, Y. Wang, J. Tam, J. Y. Howe, A. Proppe, P. Todorović, F. Li, T. T. Zhuang, C. M. Gabardo, A. R. Kirmani, C. McCallum, S. F. Hung, Y. Lum, M. Luo, Y. Min, A. Xu, C. P. O'Brien, B. Stephen, B. Sun, A. H. Ip, L. J. Richter, S. O. Kelley, D. Sinton, and E. H. Sargent, Efficient electrically powered CO_2-to-ethanol via suppression of deoxygenation, *Nat. Energy* 5(6), 478 (2020)
17. P. An, L. Wei, H. Li, B. Yang, K. Liu, J. Fu, H. Li, H. Liu, J. Hu, Y. R. Lu, H. Pan, T. S. Chan, N. Zhang, and M. Liu, Enhancing CO_2 reduction by suppressing hydrogen evolution with polytetrafluoroethylene protected copper nanoneedles, *J. Mater. Chem. A* 8(31), 15936 (2020)
18. H. Zhou, K. Liu, H. Li, M. Cao, J. Fu, X. Gao, J. Hu, W. Li, H. Pan, J. Zhan, Q. Li, X. Qiu, and M. Liu, Recent advances in different-dimension electrocatalysts for carbon dioxide reduction, *J. Colloid Interface Sci.* 550, 17 (2019)
19. Y. Zhou, F. Che, M. Liu, C. Zou, Z. Liang, P. De Luna, H. Yuan, J. Li, Z. Wang, H. Xie, H. Li, P. Chen, E. Bladt, R. Quintero-Bermudez, T. K. Sham, S. Bals, J. Hofkens, D. Sinton, G. Chen, and E. H. Sargent, Dopant-induced electron localization drives CO_2 reduction to C_2 hydrocarbons, *Nat. Chem.* 10(9), 974 (2018)
20. S. Nitopi, E. Bertheussen, S. B. Scott, X. Liu, A. K. Engstfeld, S. Horch, B. Seger, I. E. L. Stephens, K. Chan, C. Hahn, J. K. Norskov, T. F. Jaramillo, and I. Chorkendorff, Progress and perspectives of electrochemical CO_2 reduction on copper in aqueous electrolyte, *Chem. Rev.* 119(12), 7610 (2019)
21. Y. Y. Birdja, E. Pérez-Gallent, M. C. Figueiredo, A. J. Göttle, F. Calle-Vallejo, and M. T. M. Koper, Advances and challenges in understanding the electrocatalytic conversion of carbon dioxide to fuels, *Nat. Energy* 4(9), 732 (2019)
22. W. Luo, X. Nie, M. J. Janik, and A. Asthagiri, Facet dependence of CO_2 reduction paths on Cu electrodes, *ACS Catal.* 6(1), 219 (2016)
23. H. Li, F. Calle-Vallejo, M. J. Kolb, Y. Kwon, Y. Li, and M. T. Koper, Why (1 0 0) terraces break and make bonds: Oxidation of dimethyl ether on platinum single-crystal electrodes, *J. Am. Chem. Soc.* 135(38), 14329 (2013)
24. M. T. Koper, Structure sensitivity and nanoscale effects in electrocatalysis, *Nanoscale* 3(5), 2054 (2011)
25. X. G. Zhang, S. Feng, C. Zhan, D. Y. Wu, Y. Zhao, and Z. Q. Tian, Electroreduction reaction mechanism of carbon dioxide to C_2 products via Cu/Au bimetallic catalysis: A theoretical prediction, *J. Phys. Chem. Lett.* 11(16), 6593 (2020)
26. Z. X. Chen, K. M. Neyman, A. B. Gordienko, and N. Rösch, Surface structure and stability of PdZn and PtZn alloys: Density-functional slab model studies, *Phys. Rev. B* 68(7), 075417 (2003)
27. D. Kim, J. Resasco, Y. Yu, A. M. Asiri, and P. Yang, Synergistic geometric and electronic effects for electrochemical reduction of carbon dioxide using gold-copper bimetallic nanoparticles, *Nat. Commun.* 5(1), 4948 (2014)
28. A. Nilsson, L. G. M. Pettersson, B. Hammer, T. Bligaard, C. H. Christensen, and J. K. Nørskov, The electronic structure effect in heterogeneous catalysis, *Catal. Lett.* 100(3–4), 111 (2005)
29. J. K. Norskov, F. Abild-Pedersen, F. Studt, and T. Bligaard, Density functional theory in surface chemistry and catalysis, *Proc. Natl. Acad. Sci. USA* 108(3), 937 (2011)
30. M. Luo, Z. Wang, Y. C. Li, J. Li, F. Li, Y. Lum, D. H. Nam, B. Chen, J. Wicks, A. Xu, T. Zhuang, W. R. Leow, X. Wang, C. T. Dinh, Y. Wang, Y. Wang, D. Sinton, and E. H. Sargent, Hydroxide promotes carbon dioxide electroreduction to ethanol on copper via tuning of adsorbed hydrogen, *Nat. Commun.* 10(1), 5814 (2019)
31. A. Bagger, W. Ju, A. S. Varela, P. Strasser, and J. Rossmeisl, Electrochemical CO_2 reduction: A classification problem, *ChemPhysChem* 18(22), 3266 (2017)
32. Y. Zheng, A. Vasileff, X. Zhou, Y. Jiao, M. Jaroniec, and S. Z. Qiao, Understanding the roadmap for electrochemical reduction of CO_2 to multi-carbon oxygenates and hydrocarbons on copper-based catalysts, *J. Am. Chem. Soc.* 141(19), 7646 (2019)
33. Z. Zhao and G. Lu, Computational screening of near-surface alloys for CO_2 electroreduction, *ACS Catal.* 8(5), 3885 (2018)
34. S. Lee, G. Park, and J. Lee, Importance of Ag–Cu biphasic boundaries for selective electrochemical reduction of CO_2 to ethanol, *ACS Catal.* 7(12), 8594 (2017)
35. X. Lv, L. Shang, S. Zhou, S. Li, Y. Wang, Z. Wang, T. K. Sham, C. Peng, and G. Zheng, Electron-deficient Cu sites on Cu_3Ag_1 catalyst promoting CO_2 electroreduction to alcohols, *Adv. Energy Mater.* 10(37), 2001987 (2020)
36. D. Ren, B. S. H. Ang, and B. S. Yeo, Tuning the selectivity of carbon dioxide electroreduction toward ethanol on oxide-derived Cu_xZn catalysts, *ACS Catal.* 6(12), 8239 (2016)
37. H. S. Jeon, J. Timoshenko, F. Scholten, I. Sinev, A. Herzog, F. T. Haase, and B. R. Cuenya, Operando insight into the correlation between the structure and composition of CuZn nanoparticles and their selectivity for the electrochemical CO_2 reduction, *J. Am. Chem. Soc.* 141(50), 19879 (2019)
38. A. R. Paris and A. B. Bocarsly, Ni–Al films on glassy carbon electrodes generate an array of oxygenated organics from CO_2, *ACS Catal.* 7(10), 6815 (2017)
39. A. R. Paris and A. B. Bocarsly, Mechanistic insights into C_2 and C_3 product generation using Ni_3Al and Ni_3Ga electrocatalysts for CO_2 reduction, *Faraday Discuss.* 215, 192 (2019)
40. D. A. Torelli, S. A. Francis, J. C. Crompton, A. Javier, J. R. Thompson, B. S. Brunschwig, M. P. Soriaga, and N. S. Lewis, Nickel–gallium-catalyzed electrochemical reduction of CO_2 to highly reduced products at low overpotentials, *ACS Catal.* 6(3), 2100 (2016)
41. R. Kortlever, I. Peters, C. Balemans, R. Kas, Y. Kwon, G. Mul, and M. T. Koper, Palladium-gold catalyst for the electrochemical reduction of CO_2 to C_1–C_5 hydrocarbons, *Chem. Commun. (Camb.)* 52(67), 10229 (2016)

42. K. J. P. Schouten, E. Pérez Gallent, and M. T. M. Koper, Structure sensitivity of the electrochemical reduction of carbon monoxide on copper single crystals, *ACS Catal.* 3(6), 1292 (2013)
43. H. A. Hansen, C. Shi, A. C. Lausche, A. A. Peterson, and J. K. Norskov, Bifunctional alloys for the electroreduction of CO_2 and CO, *Phys. Chem. Chem. Phys.* 18(13), 9194 (2016)
44. M. J. Cheng, E. L. Clark, H. H. Pham, A. T. Bell, and M. Head-Gordon, Quantum mechanical screening of single-atom bimetallic alloys for the selective reduction of CO_2 to C_1 hydrocarbons, *ACS Catal.* 6(11), 7769 (2016)
45. A. Vasileff, C. Xu, Y. Jiao, Y. Zheng, and S. Z. Qiao, Surface and interface engineering in copper-based bimetallic materials for selective CO_2 electroreduction, *Chem* 4(8), 1809 (2018)
46. M. Karamad, V. Tripkovic, and J. Rossmeisl, Intermetallic alloys as CO electroreduction catalysts — Role of isolated active sites, *ACS Catal.* 4(7), 2268 (2014)
47. Y. Cai and X. Luo, First-principles investigation of carbon dioxide adsorption on MN_4 doped graphene, *AIP Adv.* 10(12), 125013 (2020)
48. A. C. Hegde, K. Venkatakrishna, and N. Eliaz, Electrodeposition of Zn–Ni, Zn–Fe and Zn–Ni–Fe alloys, *Surf. Coat. Tech.* 205(7), 2031 (2010)
49. G. Kresse and J. Hafner, *Ab initio* molecular-dynamics simulation of the liquid-metal-amorphous-semiconductor transition in germanium, *Phys. Rev. B* 49(20), 14251 (1994)
50. G. Kresse and J. Furthmüller, Efficient iterative schemes for *ab initio* total-energy calculations using a plane-wave basis set, *Phys. Rev. B* 54(16), 11169 (1996)
51. G. Kresses and J. Hafner, Efficiency of *ab-initio* total energy calculations for metals and semiconductors using a plane-wave basis set, *Comput. Mater. Sci.* 6(1), 15 (1996)
52. J. P. Perdew, J. A. Chevary, S. H. Vosko, K. A. Jackson, M. R. Pederson, D. J. Singh, and C. Fiolhais, Atoms, molecules, solids, and surfaces: Applications of the generalized gradient approximation for exchange and correlation, *Phys. Rev. B* 46(11), 6671 (1992)
53. K. Liu, J. Fu, L. Zhu, X. Zhang, H. Li, H. Liu, J. Hu, and M. Liu, Single-atom transition metals supported on black phosphorene for electrochemical nitrogen reduction, *Nanoscale* 12(8), 4903 (2020)
54. J. K. Nörskov, T. Bligaard, J. Rossmeisl, and C. H. Christensen, Towards the computational design of solid catalysts, *Nat. Chem.* 1(1), 37 (2009)
55. J. Li, Z. Wang, C. McCallum, Y. Xu, F. Li, Y. Wang, C. M. Gabardo, C. T. Dinh, T. T. Zhuang, L. Wang, J. Y. Howe, Y. Ren, E. H. Sargent, and D. Sinton, Constraining CO coverage on copper promotes high-efficiency ethylene electroproduction, *Nat. Catal.* 2(12), 1124 (2019)
56. T. K. Todorova, M. W. Schreiber, and M. Fontecave, Mechanistic understanding of CO_2 reduction reaction (CO_2RR) toward multicarbon products by heterogeneous copper-based catalysts, *ACS Catal.* 10(3), 1754 (2020)
57. D. D. Zhu, J. L. Liu, and S. Z. Qiao, Recent advances in inorganic heterogeneous electrocatalysts for reduction of carbon dioxide, *Adv. Mater.* 28(18), 3423 (2016)
58. S. Hanselman, M. T. M. Koper, and F. Calle-Vallejo, Computational comparison of late transition metal (100) surfaces for the electrocatalytic reduction of CO to C_2 species, *ACS Energy Lett.* 3(5), 1062 (2018)